

# Cooling and societal change during the Late Antique Little Ice Age from 536 to around 660 AD

Ulf Büntgen<sup>1,2,3\*</sup>, Vladimir S. Myglan<sup>4</sup>, Fredrik Charpentier Ljungqvist<sup>5,6</sup>, Michael McCormick<sup>7</sup>, Nicola Di Cosmo<sup>8</sup>, Michael Sigl<sup>2,9</sup>, Johann Jungclaus<sup>10</sup>, Sebastian Wagner<sup>11</sup>, Paul J. Krusic<sup>12</sup>, Jan Esper<sup>13</sup>, Jed O. Kaplan<sup>14</sup>, Michiel A. C. de Vaan<sup>15</sup>, Jürg Luterbacher<sup>16</sup>, Lukas Wacker<sup>17</sup>, Willy Tegel<sup>18</sup> and Alexander V. Kirilyanov<sup>4,19</sup>

**Climatic changes during the first half of the Common Era have been suggested to play a role in societal reorganizations in Europe<sup>1,2</sup> and Asia<sup>3,4</sup>. In particular, the sixth century coincides with rising and falling civilizations<sup>1-6</sup>, pandemics<sup>7,8</sup>, human migration and political turmoil<sup>8-13</sup>. Our understanding of the magnitude and spatial extent as well as the possible causes and concurrences of climate change during this period is, however, still limited. Here we use tree-ring chronologies from the Russian Altai and European Alps to reconstruct summer temperatures over the past two millennia. We find an unprecedented, long-lasting and spatially synchronized cooling following a cluster of large volcanic eruptions in 536, 540 and 547 AD (ref. 14), which was probably sustained by ocean and sea-ice feedbacks<sup>15,16</sup>, as well as a solar minimum<sup>17</sup>. We thus identify the interval from 536 to about 660 AD as the Late Antique Little Ice Age. Spanning most of the Northern Hemisphere, we suggest that this cold phase be considered as an additional environmental factor contributing to the establishment of the Justinian plague<sup>7,8</sup>, transformation of the eastern Roman Empire and collapse of the Sasanian Empire<sup>12,5</sup>, movements out of the Asian steppe and Arabian Peninsula<sup>8,11,12</sup>, spread of Slavic-speaking peoples<sup>9,10</sup> and political upheavals in China<sup>13</sup>.**

Annually resolved and absolutely dated insight into late Holocene climate variability is crucial to distinguish anthropogenic from natural forced variation<sup>18</sup>, and to evaluate the performance of climate model simulations<sup>19</sup>. Spatially well-distributed palaeoclimatic archives are also essential for answering questions surrounding possible relationships between climate variability and human history<sup>5,6</sup>. However, at present, there are globally only 13 temperature-sensitive tree-ring chronologies that span the entire AD (Supplementary Table 1).

Absence of precise climate reconstructions for large parts of central Asia has impeded accurate assessment of environmental factors that may have driven momentous interactions between steppe pastoralists and peripheral sedentary civilizations. At the same time, summer warmth between June and August (JJA)

is known to control tree-ring formation at higher altitudes in the Altai Mountains<sup>20</sup>, where continental climate supports the preservation of dead wood on the ground. Despite a long history of habitation by pastoral nomads<sup>21</sup>, >60% of this region is still forested, with Siberian larch (*Larix sibirica* Ldb.) being the dominant species. Although widespread steppe environments constitute an enzootic wildlife reservoir for the plague bacterium *Yersinia pestis*<sup>22</sup>, it remains unclear whether historical pandemics in Europe originated from natural infection foci in Asia<sup>23</sup>, and what role climate might have played in their epidemic onset. Moreover, root causes for human migrations out of the central Asian steppes between the fourth and seventh centuries AD have not been unambiguously identified<sup>3,4</sup>.

Here, we present tree-ring width (TRW) samples from 152 living and 508 relict larch specimens collected at five high-elevation sites in the Russian Altai–Sayan Mountains (Supplementary Fig. 1 and Supplementary Table 2). All 660 TRW series share a significant fraction of common growth variability (Supplementary Fig. 2a), with their start and end dates distributed between 359 BC and 2011 AD (Supplementary Fig. 2b). This data set has a minimum replication of ten series in 98 AD and a maximum of 240 series in 1279 AD. The mean tree age is 355 years and the average annual growth rate is 0.44 mm (Supplementary Table 2). Reduced tree recruitment between ~350 and 650 AD implies cooler summers (Supplementary Fig. 2c), whereas intensified germination during medieval times, and again ~1500 AD suggests the opposite. Abundant dead wood at all sampling sites refutes disturbance from nomadic settlements and grazing by domestic animals. The cosmogenic <sup>14</sup>C radiocarbon time marker of 775 AD (ref. 24) provides independent isotopic age confirmation of the dendrochronological dates (Supplementary Fig. 3 and Supplementary Information). A wavelet power spectrum of the high-frequency Altai TRW chronology shows no sign of pulse-like disruptions (Supplementary Fig. 4), such as those caused by cyclic outbreaks of the larch budmoth (*Zeiraphera diniana* Gn.) in the European Alps<sup>25</sup>.

<sup>1</sup>Swiss Federal Research Institute WSL, CH-8903 Birmensdorf, Switzerland. <sup>2</sup>Oeschger Centre for Climate Change Research, CH-3012 Bern, Switzerland.

<sup>3</sup>Global Change Research Centre AS CR, CZ-61300 Brno, Czech Republic. <sup>4</sup>Siberian Federal University, RU-660041 Krasnoyarsk, Russia. <sup>5</sup>Department of History, Stockholm University, SE-106 91 Stockholm, Sweden. <sup>6</sup>Bolin Centre for Climate Research, Stockholm University, SE-106 91 Stockholm, Sweden.

<sup>7</sup>Initiative for the Science of the Human Past (SoHP), Harvard University, Cambridge, Massachusetts 02138, USA. <sup>8</sup>Institute for Advanced Study, School of Historical Studies, Princeton, New Jersey 08540, USA. <sup>9</sup>Paul Scherrer Institute PSI, CH-5232 Villigen, Switzerland. <sup>10</sup>Max Planck Institute for Meteorology, DE-20146 Hamburg, Germany. <sup>11</sup>Institute for Coastal Research, Helmholtz-Zentrum Geesthacht, DE-21502 Geesthacht, Germany. <sup>12</sup>Navarino Environmental Observatory, GR-24001 Messinia, Greece. <sup>13</sup>Department of Geography, Johannes Gutenberg University, DE-55099 Mainz, Germany.

<sup>14</sup>University of Lausanne, Institute of Earth Surface Dynamics, CH-1015 Lausanne, Switzerland. <sup>15</sup>Department of Linguistics and Information Sciences, University of Lausanne, CH-1015 Lausanne, Switzerland. <sup>16</sup>Department of Geography, Justus Liebig University, DE-35390 Giessen, Germany. <sup>17</sup>Laboratory for Ion Beam Physics, ETHZ, CH-8093 Zurich, Switzerland. <sup>18</sup>Chair of Forest Growth, Albert-Ludwigs University, DE-79106 Freiburg, Germany. <sup>19</sup>VN Sukachev Institute of Forest SB RAS, RU-660036 Krasnoyarsk, Russia. \*e-mail: [buentgen@wsl.ch](mailto:buentgen@wsl.ch)

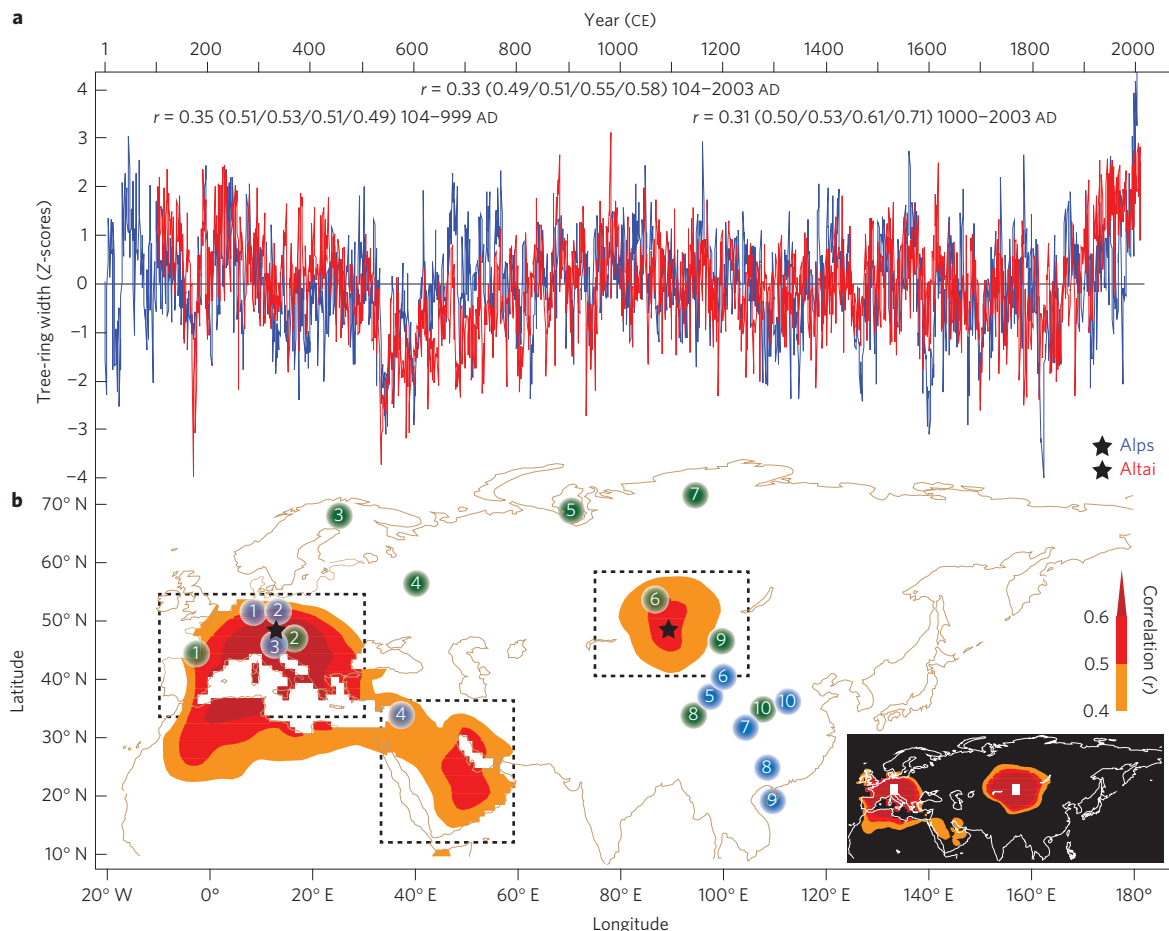


**Figure 1 | Growth coherency and climate sensitivity. a**, Normalized Alpine<sup>5</sup> and Altai regional-curve-standardized TRW chronologies (blue and red, respectively). Correlation coefficients refer to original and smoothed (20/40/80/120 yr) records plus full and split (</>1000 AD) periods. **b**, Corresponding spatial correlations (1900–2003) against gridded JJA temperatures. Locations of ten temperature (green) and hydroclimatic (blue) proxies (Supplementary Table 5), with frames indicating regions for which anthropogenic land-use changes were modelled (Supplementary Fig. 15). Inset reveals spatial correlations of gridded JJA temperatures from the Alpine (45°–50° N and 10°–15° E) and Altai (45°–50° N and 85°–90° E) records against the same gridded data set over Eurasia (Supplementary Fig. 8).

Although separated by ~7,600 km, the new Altai TRW chronology (Supplementary Information) shares remarkably high agreement with dendroclimatological findings from the Austrian Alps<sup>5</sup> (the Alpine chronology; Fig. 1a). Statistically significant ( $p < 0.001$ ) correlations between the Asian and Alpine records suggest a large-scale teleconnection pattern associated with the upper-troposphere (200 hPa) geopotential height and meridional velocity fields: the circumglobal wave train<sup>26</sup>. Coupled climate model simulations back to 850 AD (ref. 27) also reproduce covarying climate patterns in Europe and central Asia (Supplementary Fig. 5), furthermore suggesting that warm summers with anomalous high-pressure conditions most likely coincide with below-average precipitation totals across these regions (Supplementary Fig. 6).

Both TRW chronologies from the Alps and the Altai capture a substantial fraction of instrumental-based, twentieth-century regional JJA temperature variability (Supplementary Fig. 7). Significant proxy-to-target agreement at all frequency domains refutes any ‘divergence issue’ in both chronologies (Supplementary Information). Although the spatial temperature signature of the Alpine record is larger than the one from the Altai (Fig. 1b), both are nearly geographically identical to the correlation fields produced by observational JJA temperatures over the same region (Fig. 1b inset; Supplementary Fig. 8). The warmest reconstructed summer in central Asia was 982 AD (+1.6 °C with respect to 1961–1990), and six of the twelve warmest summers have occurred

since 2004 (Fig. 2a). The summer of 2010, associated with an exceptional heatwave over western Russia<sup>28</sup>, is only the twelfth warmest. The Alpine record’s warmest summer (+3.5 °C with respect to 1961–1990;  $^{\circ}\text{C}_{\text{w.r.t.1961-1990}}$ ) coincided with the European heatwave of 2003 (ref. 5; Fig. 2b). Despite slightly different uncertainty ranges (Supplementary Fig. 9), the warmest decade in both reconstructions is the most recent. The coldest central Asian and European summers are 172 and 1821 AD, respectively (−4.6 and −3.3 °C<sub>w.r.t.1961-1990</sub>). The 540s were the coldest and second coldest decade in the Altai and Alpine reconstruction, respectively (−3.2 and −1.9 °C<sub>w.r.t.1961-1990</sub>). Of the 20 coldest central Asian (European) summers, 13 (5) occurred in the sixth century after 536 AD. Thirteen (5) out of the 20 coldest decades in the Altai (Alpine) record fall in the sixth and seventh centuries.

Newly dated bipolar ice cores describe a large volcanic eruption at northern high latitudes in March 536 AD (ref. 14), which injected huge amounts of aerosol into the stratosphere (an estimated global forcing of −11.3 W m<sup>−2</sup>). Another (tropical) eruption in 540 (−19.1 W m<sup>−2</sup>) exceeded the forcing of Tambora in April 1815 (−17.2 W m<sup>−2</sup>), and was followed by a smaller but still substantial eruption in 547 (−1.1 W m<sup>−2</sup>; Fig. 2c)<sup>14</sup>. The abrupt summer cooling after this unique sequence of eruptions was probably sustained by positive feedback loops of ocean-heat content and sea-ice extension<sup>15,16</sup> (Supplementary Information), with additional forcing probably contributed by the exceptional seventh-century

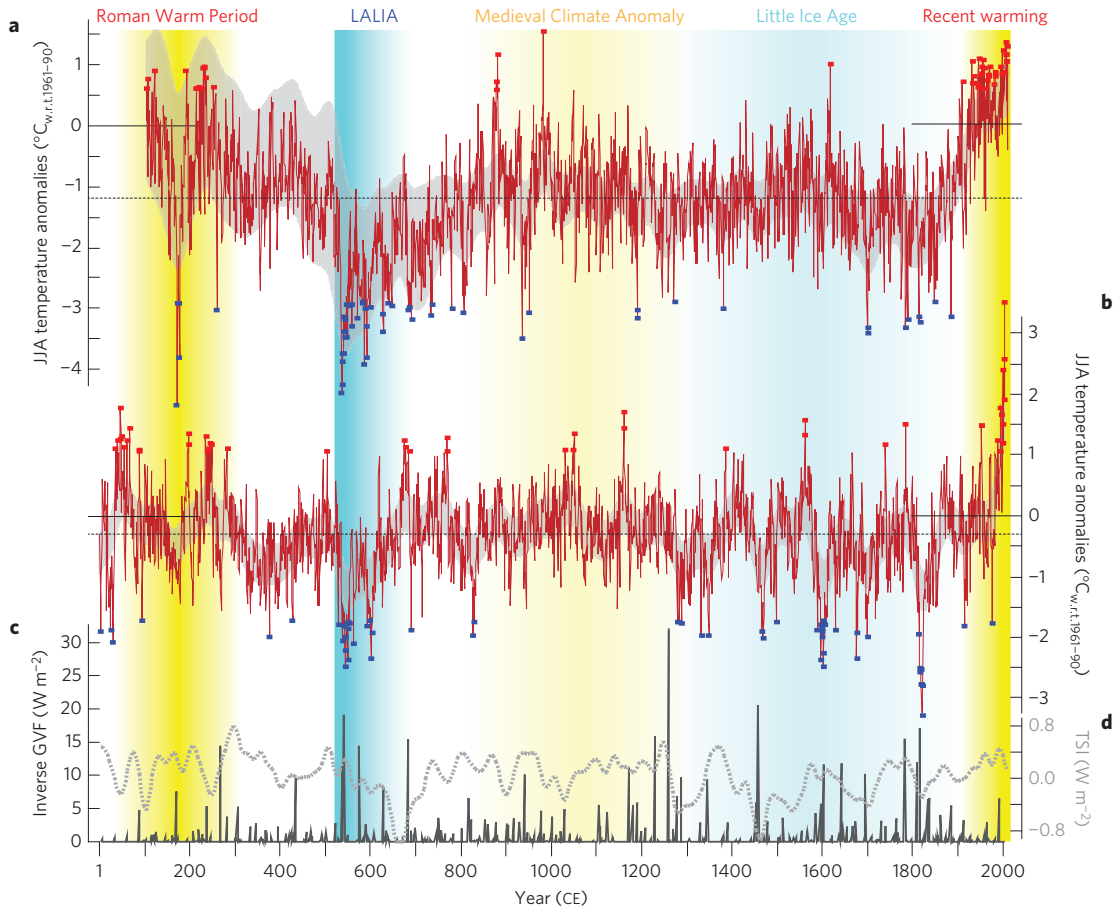


**Figure 2 | Eurasian summer temperature variability.** **a, b**, Reconstructed temperatures from the Russian Altai (**a**) and the European Alps<sup>5</sup> (**b**), with blue and red squares indicating (51/47) positive and (53/57) negative annual extremes (>2 standard deviations), respectively. Grey background shadings denote reconstruction uncertainty after 80-year low-pass filtering (Supplementary Fig. 9). **c, d**, Ice-core-derived global estimates of volcanic<sup>14</sup> (GVf; dark grey; **c**) and total solar irradiance<sup>17</sup> (TSI; light dashed grey; **d**) forcing. Black dashed lines refer to the long-term reconstruction mean of the Common Era.

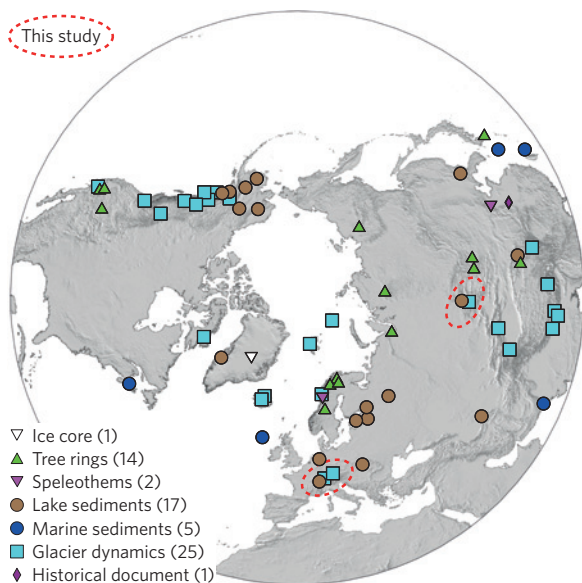


**Figure 3 | Multi-proxy large-scale evidence of the LALIA.** Compilation of 65 temperature-sensitive records from seven different types of proxy archive distributed over the extra-tropical Northern Hemisphere (>20° N). All proxy records either contain below-average values between 536 and ~660 AD or mention of a distinct cooling during this interval has been published (Supplementary Table 3).

solar minimum<sup>17</sup> (Fig. 2d). As a result, the striking cold phase from 536 to ~660 AD is hereafter termed the Late Antique Little Ice Age (LALIA). Independent evidence for this episode, which conceivably exceeded the severity of all cold events that occurred during the Little Ice Age (LIA; Fig. 2), is found in a wide range of diverse proxy archives from the Northern Hemisphere (Fig. 3 and Supplementary Table 3). Owing to changes in the Earth axis (a stronger inclination angle), extra-tropical summer short-wave insolation was higher than present day<sup>29</sup>, making the LALIA cooling even more outstanding.

Superposed epoch analyses centred on the 20 largest volcanic forcings of the AD (Supplementary Table 4) detect distinct post-eruption depressions in both the Alpine and Altai reconstructions (Supplementary Fig. 10). Sharp and immediate summer cooling was stronger under the continental climate of central Asia in comparison with Europe where ocean-induced thermal inertia has a mitigating effect. Patterns of volcanic-driven summer cooling also differ in space and time (Supplementary Fig. 11). Although the thermal shock after the cluster of eruptions in 536, 540 and 547 AD is evident in both reconstructions, the early-nineteenth-century cooling after the unnamed eruption in 1809 and Tambora in 1815 is less prominent in the Altai. Cross-spectral analysis indicates maximum coherency between the Alpine and Altai records on longer timescales (Supplementary Fig. 12), which might be explained by a Eurasian-wide wave-train-like teleconnection<sup>26,27</sup> (Supplementary Figs 5–6).

Coherent low-frequency behaviour in the Altai and Alpine records is further reflected by centennial-scale Eurasian temperature

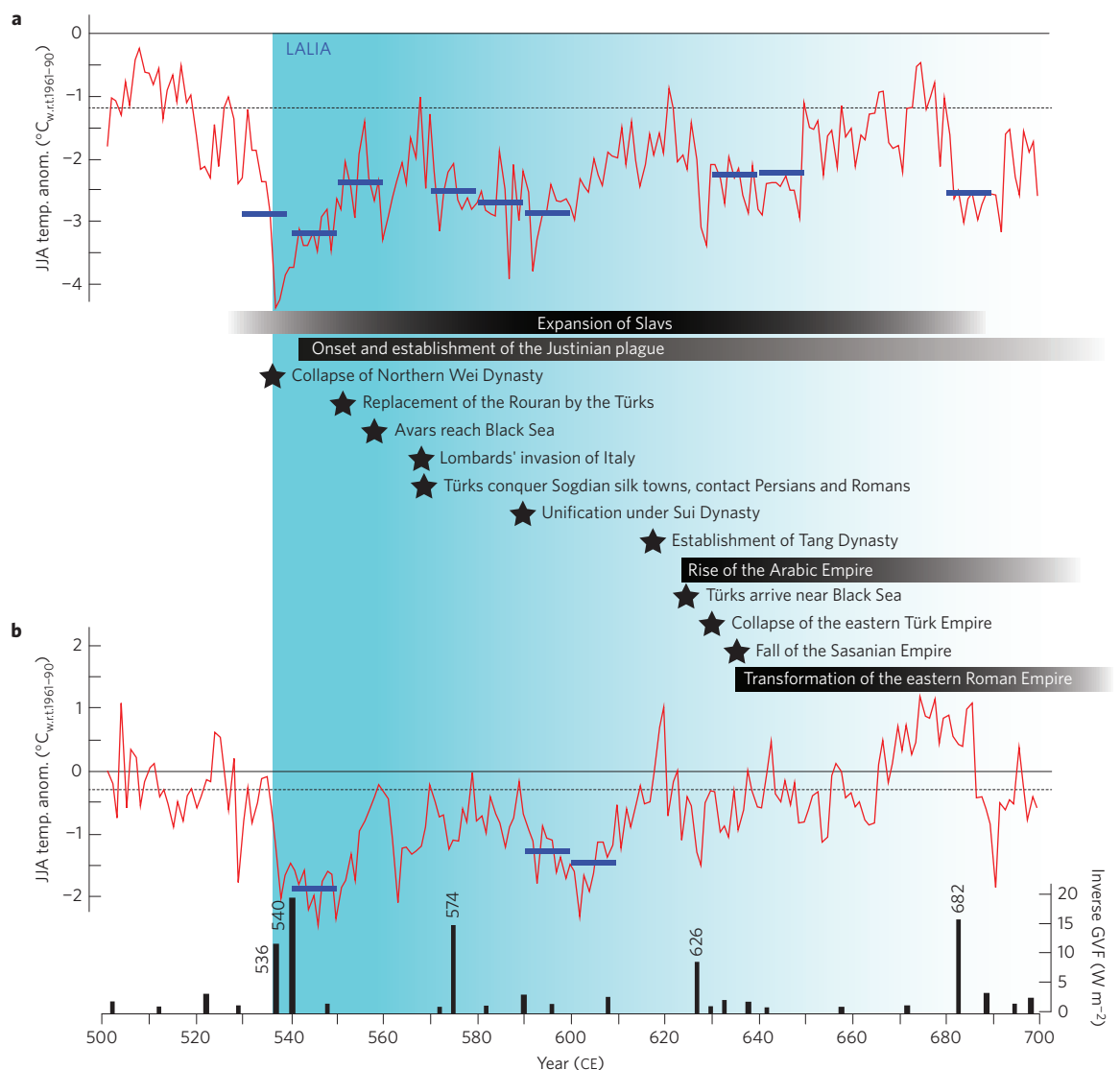


**Figure 4 | Cooling and societal change during the LALIA.** **a–c**, Reconstructed summer temperatures from the Russian Altai (**a**) and the European Alps (**b**), together with estimated volcanic forcing<sup>14</sup> (**c**). Blue lines highlight the coldest decades of the LALIA that range among the ten coldest decades of the Common Era. Horizontal bars, shadings and stars refer to major plague outbreaks, rising and falling empires, large-scale human migrations, and political turmoil (Supplementary Information). Black dashed lines refer to the long-term reconstruction mean of the Common Era.

variability (Supplementary Fig. 13a and Supplementary Table 5): The generally warmer conditions prevailing in the first centuries AD until ~300 AD, from ~800–1200 AD, and again in the twentieth century were interrupted by the LALIA and several cold events between ~1300 and 1850 AD. Independent hydroclimatic proxies from Europe and Asia describe dry conditions in the twelfth century, and from ~1400–1700 AD (Supplementary Fig. 13b). Although a long-term, pre-industrial negative temperature trend reflects the role of orbital forcing<sup>29</sup> (Supplementary Fig. 14a), this drift is less conspicuous in hydroclimate (Supplementary Fig. 14b).

Although associated with uncertainty, the LALIA—during which the fraction of pastoral and agricultural land use in central Europe and the Mediterranean seems exceptionally low (Supplementary Fig. 15)—probably exceeded the rate of change and magnitude of any other AD cold phase. The LALIA can therefore be considered as an additional environmental driver of crop failure, famine and plague, as well as a possible trigger for political, societal and economic turmoil (Fig. 4). Outbreak of the Justinian plague between 541 and 543 AD across the Later Roman Empire, as well as its subsequent pandemic development, followed widespread

food shortages right after the onset of the LALIA. Spreading apparently from Asia<sup>7</sup>, this persisting disease killed many millions of people and possibly contributed to the reduction of the eastern Roman Empire<sup>1,2</sup>. At the same time, shorter growing seasons and subsequent nutritional deficiencies in people and livestock probably initiated large-scale pastoral movements towards China (Supplementary Information).

Although the political situation in Mongolia during the sixth century is not fully understood, it is presumed that conflicts among nomadic groups and regimes in northern China culminated in the replacement of the Rouran as the dominant steppe power by the Turks in 551 AD. This suggests that there were major upheavals taking place in central Asia as early as the 550s, which gradually embroiled much of the central Eurasian steppe region, continuing into the 560s and 580s. The Avars arrived north of the Black Sea ~550 AD (Fig. 4), entered into diplomatic relations but also military conflict with the Romans, and ultimately settled in modern Hungary<sup>11</sup>. Renewed turmoil in central Asia reached the peripheral sedentary empires in the 620s. The Türk ruler Illig Qaghan raided and invaded north China in the 620s, but after 626 experienced

internal wars and Tang counterattacks, leading to the defeat and collapse of the eastern Türk Empire in 630 AD (ref. 13). The western Türks, expanding across central Asia, apparently reached the frontiers of empires east of the Black Sea where, in 625, Emperor Heraclius established diplomatic contacts with ‘Türks from the East’ (Supplementary Information). This alliance prompted the Türks’ attacks on Persia through the Caspian Gates that probably played an important role in Heraclius’s strategic victory over the Persians.

In a period partly overlapping with the LALIA, the Proto-Slavic dialects spread from a yet unknown homeland across most of continental Europe. Archaeological evidence of Slavic populations in the sixth and seventh centuries suggests that they originated in the greater Carpathian region<sup>9</sup>, but the motivation for their expansion remains unclear. Westward-moving steppe people such as the Avars, as well as opportunities for trading or developing unexploited border regions abandoned by the Roman administration, have been suggested as impetus for the movement of Slavic-speaking people<sup>10</sup>. The Avars’ arrival in Pannonia may also have reinforced the political opportunity seized by the departing Lombards who went on to invade Italy in 568 AD (ref. 30). Insofar as cooling affected the Arabian Peninsula (Fig. 1b and Supplementary Fig. 8), the expected precipitation surplus together with reduced evapotranspiration during parts of the LALIA could have boosted scrub vegetation as fodder over arid areas, and thus indirectly contributed to the rise of the Islamic Empire<sup>12</sup>. Larger camel herds may have facilitated transportation of the Arab armies and their supplies during the substantial conquests in the seventh century<sup>12</sup>, during which the reconstructed fraction of human land use seems relatively high in the Arabian Peninsula (Supplementary Fig. 15).

Although any hypothesis of a causal nexus between the volcanic-induced sixth-century unprecedented thermal shock and subsequent plague outbreaks, rising and falling empires, human migrations, and political upheaval requires caution, our newly obtained knowledge of the multidimensional impact of the LALIA fits in well with the main transformative events that occurred in Eurasia during that time. In light of a still inadequate understanding of the various push–pull factors that may have been involved in long-distance population movements, and of the role they have played in human history, our ability to bring into historical analyses what we do know about past climatological and ecological consequences is particularly relevant. To overcome reductionist approaches, the use of palaeoclimatic evidence in historical arguments has to be combined with multifactor analyses and non-deterministic explanations. Case-by-case assessment will further increase our perception of the environmental conditions under which historical events occurred.

## Methods

Methods and any associated references are available in the [online version of the paper](#).

Received 6 August 2015; accepted 7 January 2016;  
published online 8 February 2016

## References

- Gunn, J. D. (ed.) *The Years Without Summer: Tracing A.D. 536 and its Aftermath* (British Archaeological Reports International, Archaeopress, 2000).
- McCormick, M. *et al.* Climate change during and after the Roman empire: Reconstructing the past from scientific and historical evidence. *J. Interdis. Hist.* **43**, 169–220 (2012).
- Czeplédy, K. From east to west: The age of nomadic migrations in Eurasia. *Arch. Eurasiae Medii Aevi* **3**, 25–126 (1983).
- Cook, E. R. in *The Ancient Mediterranean Environment between Science and History* (ed. Harris, W. V.) 89–102 (Brill, 2013).
- Büntgen, U. *et al.* 2500 years of European climate variability and human susceptibility. *Science* **331**, 578–582 (2011).
- deMenocal, P. B. Cultural responses to climate change during the Late Holocene. *Science* **292**, 667–673 (2001).
- Harbeck, M. *et al.* *Yersinia pestis* DNA from skeletal remains from the 6<sup>th</sup> century AD reveals insights into Justinianic plague. *PLoS Pathog.* **9**, e1003349 (2013).
- Demandt, A. *Die Spätantike. Römische Geschichte von Diocletian bis Justinian 284–565 n. Chr.* (C.H. Beck, 2007).
- Barford, P. M. Slavs beyond Justinian’s frontiers. *Stud. Slavica Balcanica Petropolitana* **4**, 21–32 (2008).
- Heather, P. *Empires and Barbarians. Migration, Development and the Birth of Europe* (Pan Macmillan, 2009).
- Golden, P. in *Turko-Mongol Rulers, Cities and City Life* (ed. Durand-Guédy, D.) 21–74 (Brill, 2013).
- Kennedy, H. N. *The Armies of the Caliphs: Military and Society in the Early Islamic State* (Routledge, 2001).
- Fei, J., Zhou, J. & Hou, Y. Circa A.D. 626 volcanic eruption, climatic cooling, and the collapse of the Eastern Turkic Empire. *Climatic Change* **81**, 469–475 (2007).
- Sigl, M. *et al.* Timing and climate forcing of volcanic eruptions for the past 2,500 years. *Nature* **523**, 543–549 (2015).
- Miller, G. H. *et al.* Abrupt onset of the Little Ice Age triggered by volcanism and sustained by sea-ice/ocean feedbacks. *Geophys. Res. Lett.* **39**, L02708 (2012).
- McGregor, H. V. *et al.* Robust global ocean cooling trend for the pre-industrial Common Era. *Nature Geosci.* **8**, 671–677 (2015).
- Steinhilber, F., Beer, J. & Fröhlich, C. Total solar irradiance during the Holocene. *Geophys. Res. Lett.* **36**, L19704 (2009).
- PAGES 2k Consortium. Continental-scale temperature variability during the past two millennia. *Nature Geosci.* **6**, 339–346 (2013).
- Braconnot, P. *et al.* Evaluation of climate models using palaeoclimatic data. *Nature Clim. Change* **2**, 417–424 (2012).
- Myglan, V. S., Oidupaa, O. C. & Vaganov, E. A. A 2367-year tree-ring chronology for the Altay-Sayan region (Mongun-Taiga Mountain Massif). *Archaeol. Ethnol. Anthropol. Eurasia* **40**, 76–83 (2012).
- Agatova, A. R. *et al.* Glacier dynamics, palaeohydrological changes and seismicity in southeastern Altai (Russia) and their influence on human occupation during the last 3000 years. *Quat. Int.* **324**, 6–19 (2014).
- Kausrud, K. L. *et al.* Modeling the epidemiological history of plague in Central Asia: Palaeoclimatic forcing on a disease system over the past millennium. *BMC Biol.* **8**, 112 (2010).
- Schmid, B. V. *et al.* Climate-driven introduction of the Black Death and successive plague reintroductions into Europe. *Proc. Natl Acad. Sci. USA* **112**, 3020–3025 (2015).
- Büntgen, U. *et al.* Extra-terrestrial confirmation of tree-ring dating. *Nature Clim. Change* **4**, 404–405 (2014).
- Esper, J., Büntgen, U., Frank, D. C., Nievergelt, D. & Liebhold, A. 1200 years of regular outbreaks in alpine insects. *Proc. R. Soc. B* **274**, 671–679 (2007).
- Saeed, S., Van Lipzig, N., Müller, W. A., Saeed, F. & Zanchettin, D. Influence of the circumglobal wave-train on European summer precipitation. *Clim. Dynam.* **43**, 503–515 (2014).
- Jungclaus, J. H., Lohmann, K. & Zanchettin, D. Enhanced 20th-century heat transfer to the Arctic simulated in the context of climate variations over the last millennium. *Clim. Past* **10**, 2201–2213 (2014).
- Barriopedro, D., Fischer, E. M., Luterbacher, J., Trigo, R. M. & García-Herrera, R. The hot summer of 2010: redrawing the temperature record map of Europe. *Science* **332**, 220–224 (2011).
- Esper, J. *et al.* Orbital forcing of tree-ring data. *Nature Clim. Change* **2**, 862–866 (2012).
- Pohl, W. *Die Awaren: ein Steppenvolk in Mitteleuropa 567–822 n. Chr.* (C.H. Beck, 1988).

## Acknowledgements

B. Bramanti, B. M. S. Campbell, S. M. Hsiang and C. Oppenheimer kindly commented on earlier versions of this article. D. Galvan helped with the radiocarbon measurements (within the WSL-internal COSMIC project), L. Hellmann provided technical support for Fig. 4 (through the E. Mayr-Stihl Foundation), and D. Zanchettin contributed insight on positive feedback loops. Ü.B. was supported by the Czech project ‘Building up a multidisciplinary scientific team focused on drought’ (No. CZ.1.07/2.3.00/20.0248). J.O.K. was supported by the European Research Council (COEVOLVE 313797), and J.J., S.W. and J.L. acknowledge the German Science Foundation project ‘Attribution of forced and internal Chinese climate variability in the common era’. This study was conducted within the interdisciplinary and international framework of the PAGES initiative (Euro-Med 2k and Asia-2k), which in turn received support from the US and Swiss National Science Foundations, US National Oceanographic and Atmospheric Administration and by the International Geosphere-Biosphere Programme. Tree-ring data from the Altai were collected and measured through support from the Russian Science Foundation (project 14-14-00295). Historical evidence was extracted from work ongoing at SoHP, Harvard University.

**Author contributions**

U.B. designed the study, together with M.M., and U.B. performed most of the analyses with support from all authors. V.S.M. and A.V.K. conducted fieldwork in the Russian Altai and developed the corresponding tree-ring chronologies. M.M., N.D.C., J.O.K., M.A.C.d.V. and F.C.L. added historical insight. J.J. and S.W. provided model output, and L.W. measured and analysed  $^{14}\text{C}$ . F.C.L. compiled multi-proxy LALIA evidence for the Northern Hemisphere. U.B. wrote the paper together with F.C.L., M.M., N.D.C., P.J.K., J.E., J.L. and W.T. All authors edited the various manuscript versions and contributed to long-lasting discussions.

**Additional information**

Supplementary information is available in the online version of the paper. Reprints and permissions information is available online at [www.nature.com/reprints](http://www.nature.com/reprints). Correspondence and requests for materials should be addressed to U.B. and, concerning the historical component of this work, to M.M. ([sohp@fas.harvard.edu](mailto:sohp@fas.harvard.edu)).

**Competing financial interests**

The authors declare no competing financial interests.

## Methods

**Tree-ring sampling.** All 660 TRW samples were collected from living or dead larch (*Larix sibirica* Ldb.) trees at five high-elevation, near-timberline, sites in the Russian Altai–Sayan Mountains. A total of 234,399 individual TRW measurements were performed and the resulting raw time series were visually and statistically cross-dated to the corresponding calendar years. Examples of the sampling sites are provided in Supplementary Fig. 1, and detailed information on the different TRW subsets as well as the subsequent chronologies is described in Supplementary Table 2. The temporal behaviour of the new TRW data set is denoted in Supplementary Fig. 2, including details on common growth variability (Supplementary Fig. 2a) and sample distribution (Supplementary Fig. 2b). Eleven annually resolved measurements of the  $^{14}\text{C}$  to  $^{12}\text{C}$  isotopic ratio between 770 and 780 AD were made as an independent, non-dendrochronological dating confirmation<sup>20</sup> of the relict Altai samples (Supplementary Information).

**Chronology development.** Alignment of the raw TRW measurement series by their innermost ring, ideally representing cambial age at the pith, facilitated the assessment of growth trends and levels. The resulting growth curves, the so-called regional curves commonly describe trends of negative exponential shape, with very little differences between the five sites and the living and relict material. Splitting the data horizontally<sup>5</sup>, into four consecutive intervals of 500 years, reveals similar growth levels after ~500 AD but slightly wider annual increments before (Supplementary Fig. 2b). An assessment of the mean segment length (MSL) and average growth rate (AGR) of the raw TRW measurement series from the five sampling sites, as well as by sample type (Supplementary Table 2), reveals an exceptionally high degree of data homogeneity in space and time. The observed similarities in AGR and consistency in the MSL/AGR association among the various data subsets denotes their compatibility also with respect to growth rates and trends. At the same time, the observed relationship between MSL and AGR in the raw TRW series emphasizes the need for tree-ring standardization (detrending) before any meaningful interpretation of externally forced variations, that is, the putative climatic signal within the larch TRW measurements must be separated from the prevailing background noise (Supplementary Information). The combined living and relict TRW chronologies from the five sites in the Altai correlate at 0.93 ( $p < 0.0001$ ) over 1486–1814 AD. Pearson's correlation coefficients

between the newly developed TRW chronologies from five sites in the Russian Altai are significantly positive over most of the last centuries (Supplementary Table 2). Moving 31-year inter-series correlations ( $Rbar$ ) between these records, from 1677 to 1992, range from 0.53 to 0.87 with a mean of 0.72 (Supplementary Fig. 4a).

**Climate sensitivity.** Growth–climate response analyses of the new Altai TRW regional curve standardization larch chronology were calculated against monthly resolved temperature means ( $^{\circ}\text{C}$ ) and precipitation totals ( $\text{mm day}^{-1}$ ) extracted from different gridded products (Supplementary Information), averaged over different spatial domains in central Asia, over different time periods during the past 100 years. All correlations with precipitation were nonsignificant, whereas a clear relationship between TRW formation and JJA temperatures was found (Supplementary Information). The growth–climate linkage was tested for temporal and spatial stability (Supplementary Fig. 7). Decadal-scale variability during the twentieth century is most obvious in the central European ( $45^{\circ}$ – $50^{\circ}$  N and  $10^{\circ}$ – $15^{\circ}$  E) JJA temperature mean (Supplementary Fig. 7a), with below-average cooling in the 1910s, a warming peak in the 1940s and a sharp increase from ~1980 onwards. The overall variability and trend in the central Asian ( $45^{\circ}$ – $50^{\circ}$  N and  $85^{\circ}$ – $90^{\circ}$  E) JJA temperature mean is, however, significantly lower and the rapid warming of the 1980s and 1990s is less distinct (Supplementary Fig. 7b).

**Historical assessment.** As the Chinese and Roman records use different names for them, the details and identifications of some of the central Asian groups in the ancient records are often confusing and controversial. Nevertheless, it is clear that political turbulence in central Asia was underway when the extreme summer cooling began, and peaked when a new political order emerged from the second half of the sixth century, deeply affecting the peripheral areas of Rome, Sasanian Persia and China. The main questions concerning the identifications mentioned in the text are provided in the Supplementary Information.

**Data availability.** The new Altai summer temperature reconstruction together with associated metadata is archived for routine public access and use ([www.ncdc.noaa.gov/data-access/paleoclimatology-data/datasets/climate-reconstruction](http://www.ncdc.noaa.gov/data-access/paleoclimatology-data/datasets/climate-reconstruction)).